materials

MDPI

Article

Successive Short- and Long-Range Magnetic Ordering in $Ba_2Mn_3(SeO_3)_6$ with Honeycomb Layers of Mn^{3+} Ions Alternating with Triangular Layers of Mn^{2+} Ions

Artem Moskin [1,2], Ekaterina Kozlyakova [1,2], Seung Hwan Chung [3], Hyun-Joo Koo [3], Myung-Hwan Whangbo [3,4] and Alexander Vasiliev [1,2,*]

[1] Department of Low Temperature Physics and Superconductivity, Lomonosov Moscow State University, Moscow 119991, Russia
[2] Functional Quantum Materials Laboratory, National University of Science and Technology "MISIS", Moscow 119049, Russia
[3] Department of Chemistry and Research Institute for Basic Sciences, Kyung Hee University, Seoul 02447, Republic of Korea
[4] Department of Chemistry, North Carolina State University, Raleigh, NC 27695-8204, USA
* Correspondence: vasil@mig.phys.msu.ru

Abstract: Mixed-valent $Ba_2Mn^{2+}Mn_2{}^{3+}(SeO_3)_6$ crystallizes in a monoclinic $P2_1/c$ structure and has honeycomb layers of Mn^{3+} ions alternating with triangular layers of Mn^{2+} ions. We established the key parameters governing its magnetic structure by magnetization M and specific heat C_p measurements. The title compound exhibits a close succession of a short-range correlation order at T_{corr} = 10.1 ± 0.1 K and a long-range Néel order at T_N = 5.7 ± 0.1 K, and exhibits a metamagnetic phase transition at $T < T_N$ with hysteresis most pronounced at low temperatures. The causes for these observations were found using the spin exchange parameters evaluated by density functional theory calculations. The title compound represents a unique case in which uniform chains of integer spin Mn^{3+} (S = 2) ions interact with those of half-integer spin Mn^{2+} (S = 5/2) ions.

Keywords: honeycomb lattice; triangular lattice; long-range magnetic order; short-range magnetic order; first principles' calculations

Citation: Moskin, A.; Kozlyakova, E.; Chung, S.H.; Koo, H.-J.; Whangbo, M.-H.; Vasiliev, A. Successive Short- and Long-Range Magnetic Ordering in $Ba_2Mn_3(SeO_3)_6$ with Honeycomb Layers of Mn^{3+} Ions Alternating with Triangular Layers of Mn^{2+} Ions. *Materials* **2023**, *16*, 2685. https://doi.org/10.3390/ma16072685

Academic Editor: Denis Vinnik

Received: 4 March 2023
Revised: 22 March 2023
Accepted: 26 March 2023
Published: 28 March 2023

1. Introduction

Compounds of transition metal magnetic ions exhibit a wide range of phenomena, which are commonly grouped in terms of their spin values: quantum magnetism for systems of small spins and classical magnetism for systems of large spins. In both groups, the ground state that a magnetic compound reaches at low temperatures is governed largely by the dimensionality of its spin exchange interactions and also by the degree of geometrical spin frustration (hereafter, spin frustration) [1]. It quickly becomes complicated to analyze the properties of a magnetic system with magnetic ions of two (or more) different oxidation states and two (or more) different values of spins in terms of these two factors unless the relative values of its various spin exchanges are known. These days, it has become almost routine to determine the values of spin exchanges for any complex magnetic system by performing energy mapping analysis [2–4]. This method employs a number of broken-symmetry spin states of a given magnetic system, then evaluates their energies using a spin Hamiltonian made up of the spin exchanges, in addition using density functional theory (DFT) calculations and finally maps the relative energies of the broken-symmetry states from the spin Hamiltonian to those of the DFT calculations. In other words, this method relates the energy spectrum of a model Hamiltonian to that of an electronic Hamiltonian using a set of broken-symmetry states. Over the years, the energy mapping analysis has led to correct spin lattice models with which to understand the properties of numerous magnetic materials.

Among low-dimensional mixed-valent compounds of small spin, $LiCu_2O_2$ attracts attention as a type-II multiferroic since the formation of the long-range spiral magnetic order is accompanied by the emergence of ferroelectricity [5,6]. Another low-spin mixed-valent compound is NaV_2O_5 which undergoes a charge ordering transition, which gives rise to a spin gap in the magnetic excitation spectrum [7]. Among low-dimensional mixed-valent compounds of large spin, manganese-based systems are most extensively studied. Two magnetic orderings and a spin–flop transition were observed in the mixed-valent compound $Mn_3O(SeO_3)_3$, the magnetic ion arrangement of which shows the intersection of octa-kagomé spin sublattices and staircase-kagomé spin sublattices [8]. The hollandite-type compound, $Ba_{1.2}Mn_8O_{16}$, undergoes a magnetic transition at 40 K, which is significantly lower than the Weiss temperature of −385 K, a characteristic feature of high spin frustration. Strong spin frustration usually results from triangular arrangements of magnetic ions with antiferromagnetic spin exchange for each edge and/or competing ferromagnetic and antiferromagnetic interactions [9].

In the present work, we examine how to understand the magnetic properties of the mixed-valent manganese compound $Ba_2Mn^{2+}Mn^{3+}{}_2(SeO_3)_6$ [10]. In general, spin exchanges between transition-metal magnetic ions M forming ML_n polyhedra with surrounding main-group ligands L are classified into M-L-M and M-L ... L-M types [2–4], and the latter are further differentiated depending on whether or not the L ... L bridge is coordinated by a metal cation A^{m+} to form L ... A^{m+} ... L. In cases when a metal cation is present, the M-L ... A^{m+} ... L-M exchanges are further differentiated by whether or not the A^{m+} cation is a d^0 transition-metal cation or a main-group cation. The spin exchanges involving a main-group cation are almost impossible to predict using simple qualitative arguments, especially when this cation makes strong covalent bonds with the ligand to form a molecular anion, e.g., a $P_2S_6{}^{4-}$ anion in MPS_3 (M = Mn, Fe, Co, Ni) [11]. Such is the case for the $SeO_3{}^{2-}$ anion of $Ba_2Mn_3(SeO_3)_6$. As will be described below, the spin exchanges of $Ba_2Mn_3(SeO_3)_6$ are all of the Mn-O ... Se^{4+} ... O-Mn type; that is, none involves the Mn-O-Mn type so that the Mn^{3+} and Mn^{2+} ions of $Ba_2Mn_3(SeO_3)_6$ do not generate double exchanges [12]. The Mn^{2+} ions of $Ba_2Mn_3(SeO_3)_6$ form chains, with the Mn^{3+} ions in the same direction. Between these chains, triangular arrangements of the magnetic ions such as (Mn^{2+}, Mn^{2+}, Mn^{3+}) and (Mn^{2+}, Mn^{3+}, Mn^{3+}) occur in all three directions, so one might consider the presence of strong spin frustration and exhibit magnetic properties expected for a low-dimensional antiferromagnetic material. To interpret these seemingly puzzling aspects of $Ba_2Mn_3(SeO_3)_6$, we determine its spin exchanges using the energy-mapping analysis to find the cause for its low-dimension antiferromagnetic behavior.

2. Materials and Methods

Mixed-valent $Ba_2Mn^{2+}Mn_2{}^{3+}(SeO_3)_6$ was synthesized by a hydrothermal reaction of $BaCO_3$ (2 mmol), $MnCl_2{\cdot}4H_2O$ (1 mmol) and H_2SeO_3 (3 mmol) as precursors with 1.5 mL of 65% HNO_3 and 3 mL of water added. The mixture was placed into a Teflon chamber of a steel autoclave (10 mL) after the degassing was finished. The autoclave then was placed into the furnace, where the temperature was raised to 200 °C for 1 week. After this, the brown powder of $Ba_2Mn_3(SeO_3)_6$ was rinsed with water to wash out the contaminants. The obtained powder sample was found to crystallize in the monoclinic $P2_1/c$ space group with a = 5.4717(3) Å, b = 9.0636(4) Å, c = 17.6586(9) Å, β = 94.519(1), V = 873.03(8) Å^3, Z = 2 in agreement with the original solution [10] and its powder XRD pattern (BRUKER D8 Advance diffractometer Cu Kα, λ = 1.54056, 1.54439 Å, LYNXEYE detector) is shown in Figure 1.

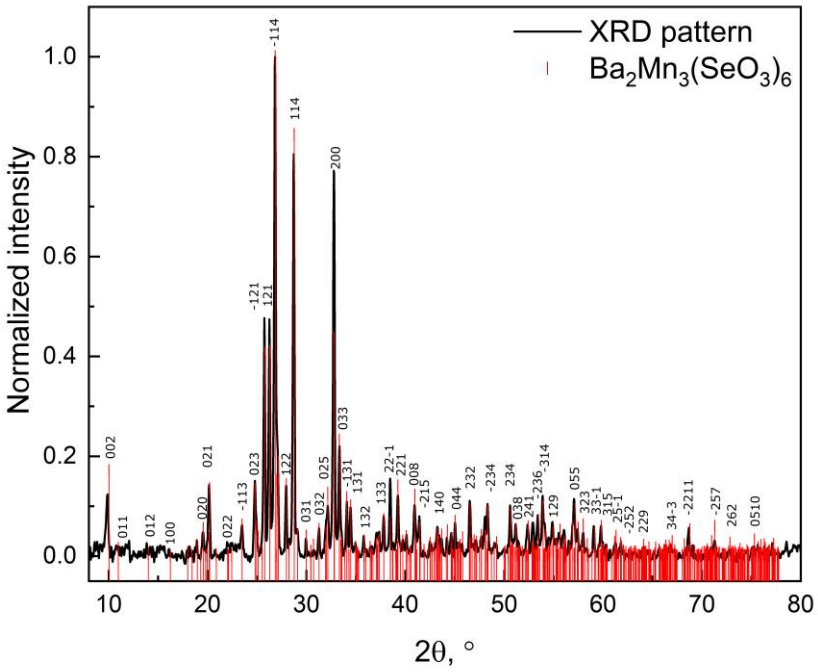

Figure 1. Diffraction pattern obtained for powder samples of $Ba_2Mn_3(SeO_3)_6$. The red lines are shown as the reference for peak positions and indexing (some of the indexes were omitted due to high density of peaks).

As depicted in Figure 2a, the structure is composed of MnO_6 octahedra interlinked with SeO_3 pyramids. The $Mn1O_6$ octahedra of Mn^{2+} ($S = 5/2$) ions form trigonal layers, and $Mn2O_6$ octahedra of Mn^{3+} ($S = 2$) ions form honeycomb layers, as shown in Figure 2b,c.

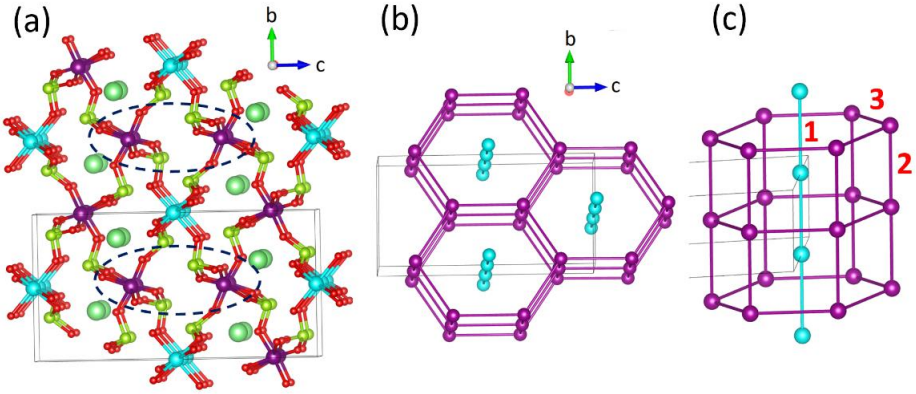

Figure 2. (**a**) The crystal structure of $Ba_2Mn_3(SeO_3)_6$, where the Mn1 and Mn2 atoms are represented by cyan and violet spheres, respectively, and the Ba and Se atoms by large and small green spheres, respectively. The $Mn2O_6$ octahedra encircled by dashed ellipses have no interlinking by a SeO_3 pyramid. (**b**) The arrangements of the Mn1 and Mn2 atoms in $Ba_2Mn_3(SeO_3)_6$. (**c**) One hexagonal prism of Mn^{3+} ions containing one chain of Mn^{2+} ions. The number 1 refers to the spin exchange J_1 of the chain of Mn^{2+} ions, while 2 and 3 refer, respectively, to spin exchanges J_2 and J_3 of the hexagonal prism of Mn^{3+} ions (see below).

Physical properties of $Ba_2Mn_3(SeO_3)_6$ were characterized by measuring the magnetization M and the specific heat C_p on ceramic samples (well-pressed pellets of 3 mm in diameter and 1 mm in thickness) using various options of "Quantum Design" Physical Properties Measurements System PPMS—9 T taken in the range 2–300 K under magnetic field $\mu_0 H$ up to 9 T.

3. Results

3.1. Magnetic Susceptibility

The magnetic susceptibility $\chi = M/H$ of $Ba_2Mn_3(SeO_3)_6$ taken at $\mu_0 H = 0.1$ T in the field-cooled regime is shown in Figure 3. In the high-temperature region, it follows the Curie–Weiss law:

$$\chi = \frac{C}{T - \theta} + \chi_0 \quad (1)$$

with the temperature-independent term $\chi_0 = -7.6 \times 10^{-4}$ emu/mol, the Curie constant $C = 10.98$ emu K/mol and the Weiss temperature $\Theta = -27.8$ K. The value of χ_0 exceeds the sum of the Pascal constants of ions and groups constituting the title compound $\chi_{0,calc} = -3.5 \times 10^{-4}$ emu/mol [13]. This should be attributed to the effect of sample holder. The value of C somewhat exceeds the value $C_{calc} = 10.375$ emu K/mol expected under the assumption of g-factor, $g = 2$, for both the Mn^{2+} and Mn^{3+} ions. Use of $g = 2$ is reasonable for Mn^{2+} ($S = 5/2$) ions with no orbital-moment contribution, but it underestimates the g-factor for Mn^{3+} ions ($S = 2$). The negative value of the Weiss temperature Θ points to the predominance of antiferromagnetic exchange interactions at elevated temperatures. Its absolute value can be influenced by the competition of ferromagnetic and antiferromagnetic exchange interactions.

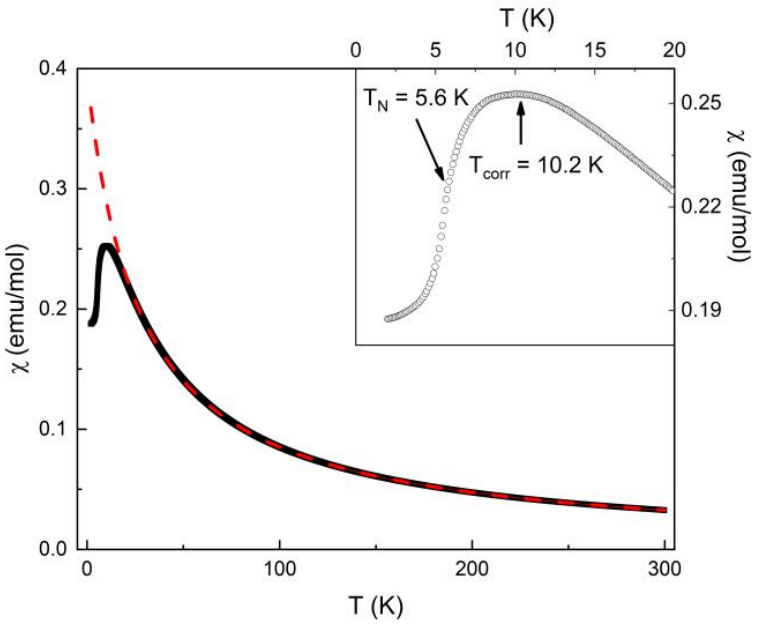

Figure 3. Temperature-dependent magnetic susceptibility χ of $Ba_2Mn_3(SeO_3)_6$ taken at $\mu_0 H = 0.1$ T in the field-cooled regime. The dashed line represents the extrapolation of the Curie–Weiss fit. The inset shows a zoomed-in view of the low temperature region of the $\chi(T)$ curve.

On lowering the temperature, the $\chi(T)$ curve passes through a broad maximum at $T_{corr} = 10.2$ K and shows a kink at $T_N = 5.6$ K, which is more pronounced in the Fisher's specific heat $d(\chi T)/dT$ (not shown). This broad maximum is typically found for a quasi-one-dimensional (1D) antiferromagnetic chain system; hence, suggesting that $Ba_2Mn_3(SeO_3)_6$ has a 1D-like antiferromagnetic subsystem. The kink at a lower temperature shows that $Ba_2Mn_3(SeO_3)_6$ undergoes a long-range antiferromagnetic order. The drop of magnetic susceptibility χ below its largest value at T_{corr} is less than one-third of that expected for a three-dimensional easy-axis antiferromagnet [14]. The absence of a so-called Curie tail at lowest temperatures signals the high chemical purity of the sample.

3.2. Field Dependence of Magnetization

The field dependencies of the magnetization M taken at selected temperatures in the $T < T_N$ and $T_N < T < T_{corr}$ regions are shown in Figure 4. At the highest temperature of our measurement, the *M(H)* curve is linear indicating that the system is in the paramagnetic state, but starts to deviate from linearity as the temperature is lowered toward T_N. Below T_N, the *M(H)* curves exhibit hysteresis, which becomes most pronounced at the lowest temperature of our measurement. In general, the Heisenberg magnets of quasi-isotropic magnetic moment experience a spin–flop transition prior to the full saturation at the spin–flip transition. This is not the case for $Ba_2Mn_3(SeO_3)_6$, although it has isotropic Mn^{2+} ions. Instead, it exhibits a metamagnetic transition inherent to the Ising magnets. Such behavior should be associated with the presence of highly anisotropic Mn^{3+} ions in the system. The well-pronounced hysteresis underlines the first-order nature of the metamagnetic transition [15].

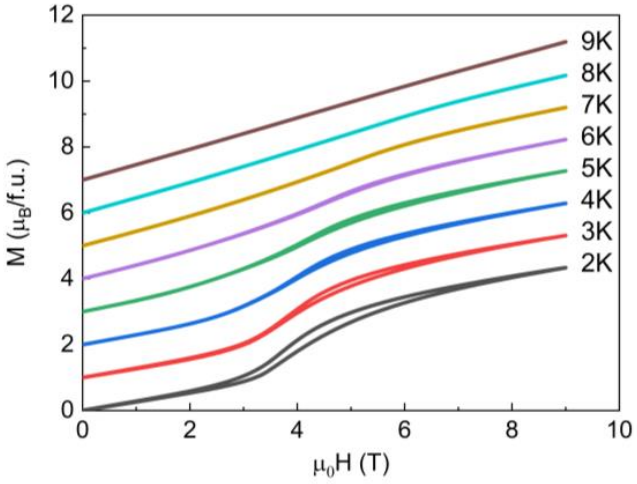

Figure 4. Magnetization curves measured for $Ba_2Mn_3(SeO_3)_6$ at selected temperature in the $T < T_N$ and $T_N < T < T_{corr}$ regions. For clarity, the curves are shifted with respect to each other by 1 μ_B/f.u.

3.3. Heat Capacity

The magnetization data are fully consistent with the specific heat data, shown in Figure 5. In a wide temperature range, the $C_p(T)$ curve can be described by the sum of the Debye function with Θ_D = 223 K and two Einstein functions with Θ_{E1} = 556 K and Θ_{E2} = 1449 K. The first of the Einstein functions can be ascribed to the oscillation mode of the MnO_6 octahedra and the second one to that of the SeO_3 pyramids. These parameters were obtained by fitting the data in the 70–290 K region with the fixed sum of the Debye and Einstein functions. The remaining data were considered as a purely magnetic contribution. Indeed, the magnetic entropy is nearly equal to the theoretical value of $R(2\ln(5) + \ln(6))$ = 41.6 J/mol K, confirming the accuracy of the fit. Nevertheless, a nonmagnetic analogue is still needed to obtain more accurate values of Debye and Einstein temperatures.

On lowering the temperature, the specific heat C_p passes through a broad maximum at T_{corr} = 10 K and shows a peak at T_N = 5.8 K. Under external magnetic field, the broad maximum retains its position, but the sharp anomaly shifts to lower temperatures. Such behavior is typical of low-dimensional antiferromagnets experiencing successive short-range and long-range orders.

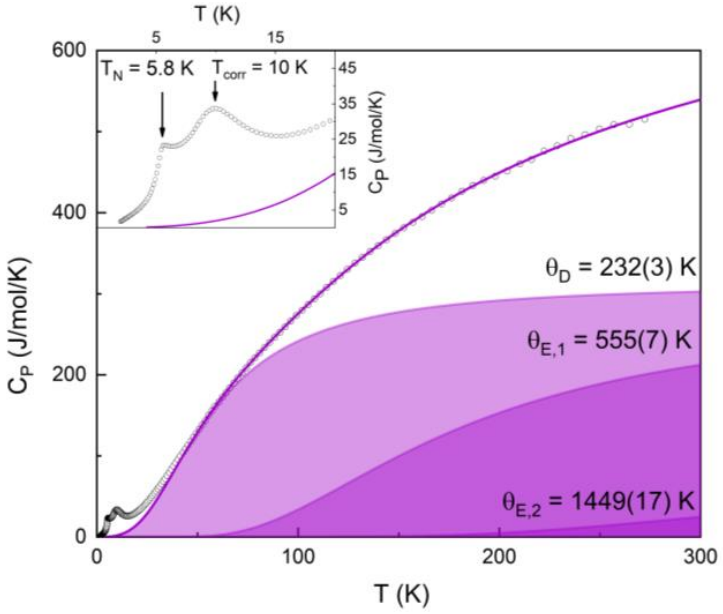

Figure 5. Temperature-dependent specific heat of $Ba_2Mn_3(SeO_3)_6$ described by the sum of Debye and two Einstein functions. The inset shows a zoomed-in view of the low temperature region along with the fitting curve.

3.4. Spin Exchanges and Interpretation

The two important issues concerning the observed magnetic properties of $Ba_2Mn_3(SeO_3)_6$ are the cause for the broad maximum of the magnetic susceptibility at T_{corr} = 10.1 ± 0.1 K, suggesting a short-range correlation as found for a 1D antiferromagnetic chain and a sharp kink at 5.7 ± 0.1 K, suggesting a long-range antiferromagnetic ordering. With $\Theta = -27.8$ K and T_N = 5.7 K (the index of spin frustration f = 5.0), the spin frustration in $Ba_2Mn_3(SeO_3)_6$ is not strong enough to prevent it from adopting a long-range antiferromagnetic ordering. This is somewhat surprising because one might expect a strong spin frustration in $Ba_2Mn_3(SeO_3)_6$. Figure 2c shows that the interaction between a chain of Mn^{2+} ions with the Mn^{3+} ions in the surrounding hexagonal prism generates numerous spin exchange triangles, which is a common arrangement leading to spin-frustration. Furthermore, these interactions must give rise to a 1D antiferromagnetic chain behavior to explain the 1D-like short range correlation at 10.1 K. To explore these issues, we first evaluate the spin exchanges of various exchange paths J in $Ba_2Mn_3(SeO_3)_6$.

All adjacent magnetic ions of $Ba_2Mn_3(SeO_3)_6$ are interconnected by the SeO_3 pyramids except for the Mn^{3+} ions encircled by dashed ellipses in Figure 2a. The O . . . O contact distances (3.988 Å) of their Mn-O . . . O-Mn exchange paths are well beyond the van der Waals distance of ~3.30 Å so these spin exchanges can be neglected. There are still numerous spin exchanges between the Mn^{2+} and Mn^{3+} ions as depicted in Figure 6a. The spin exchange paths J_2 (J_1) form chains of Mn^{3+} (Mn^{2+}) ions along the a-direction (Figure 6b). For convenience, these chains will be referred to as J_2- and J_1- chains, respectively. Note that each J_2-chain is coupled to two adjacent J_2-chains and also to two adjacent J_1-chains. Between adjacent J_1- and J_2-chains four different spin exchange paths (i.e., J_4, J_5, J_6 and J_7) occur (Figure 6c), leading to (J_1, J_4, J_5), (J_2, J_4, J_5), (J_1, J_6, J_7) and (J_2, J_6, J_7) exchange triangles. A more extended view of Figure 6c is presented in Figure S1 in the Supporting Information (SI).

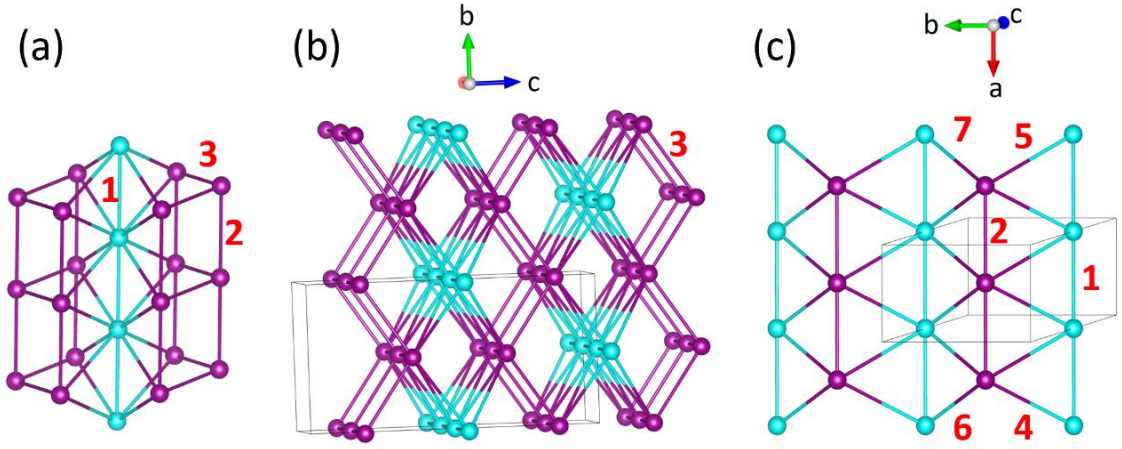

Figure 6. Arrangement of the Mn^{2+} (cyan) and Mn^{3+} (violet) ions in $Ba_2Mn_3(SeO_3)_6$, where the numbers 1–7 refer to the exchange paths J_1–J_7, respectively: (**a**) Spin exchange paths between the Mn^{2+}/Mn^{3+} ions that are bridged by the SeO_3 groups in one hexagonal prism of Mn^{3+} ions with one chain of Mn^{2+} ions. (**b**) Projection view showing how chains of Mn^{3+} ions interact with those of Mn^{2+} ions. (**c**) Spin exchange paths J_4–J_7 between the Mn^{2+} and Mn^{3+} ions.

To determine the values of these exchanges, we employ the spin Hamiltonian defined as

$$H_{spin} = -\sum_{i>j} J_{ij} \vec{S}_i \cdot \vec{S}_j, \quad (2)$$

where the spin exchange J_{ij} between two spin sites can be any one of J_1–J_7. To evaluate J_1–J_7, we carry out the energy-mapping analysis [2–4] using the eight ordered spin states, i.e., AFi, where i = 1–8, depicted in Figure S2 of the SI. First, we express the energies of the eight ordered states in terms of the spin exchanges J_1–J_7 using the spin Hamiltonian of Equation (2) and then determine the relative energies of these states (Table 1) by DFT calculations using the frozen core projector augmented plane wave [16,17] encoded in the Vienna ab Initio Simulation Package [18] and the exchange-correlation functional of Perdew, Burke and Ernzerhof [19].

Table 1. Relative energies (in meV/FU) of the eight ordered spin states obtained from DFT + U calculations.

Ordered Spin States	U_{eff} = 3 eV	U_{eff} = 4 eV
AF_1	10.01	8.27
AF_2	8.80	7.20
AF_3	6.40	5.32
AF_4	8.49	7.81
AF_5	17.84	15.03
AF_6	13.26	12.68
AF_7	3.62	3.29
AF_8	0	0

The electron correlations associated with the 3*d* states of Mn were taken into consideration by DFT + U calculations with effective on-site repulsion $U_{eff} = U - J$ = 3 eV and 4 eV [20]. All our DFT + U calculations used the plane wave cutoff energy of 450 eV, a set of (6 × 4 × 4) k-points, and the threshold of 10^{-6} eV for self-consistent-field energy convergence. Finally, the numerical values of J_1–J_7 were obtained by mapping the relative energies of the eight ordered spin states onto the corresponding energies determined by DFT + U calculations. The results of these energy-mapping analyses are summarized in Table 2.

Table 2. Geometrical parameters of the exchange paths and the values of the spin exchanges in $Ba_2Mn_3(SeO_3)_6$. The plus and minus signs of the spin exchanges represent ferromagnetic and antiferromagnetic couplings, respectively.

Path	Geometrical Parameters		Spin Exchanges (in K)	
	Ions Involved	Distance, Å	U_{eff} = 3 eV	U_{eff} = 4 eV
J_1	Mn1 . . . Mn1	5.4717	−2.23	−1.74
J_2	Mn2 . . . Mn2	5.4717	−2.62	−2.14
J_3	Mn2 . . . Mn2	5.4655	1.51	1.80
J_4	Mn1 . . . Mn2	5.9554	−2.38	−1.63
J_5	Mn1 . . . Mn2	6.0883	−0.88	−0.45
J_6	Mn1 . . . Mn2	5.9737	−2.05	−1.43
J_7	Mn1 . . . Mn2	6.1063	3.88	3.56

As already pointed out, each J_2-chain interacts with two adjacent J_2-chains and with two adjacent J_1-chains (Figure 6b). In terms of the spin exchanges of Table 2, the nature of these interchain interactions can be stated as follows:

(1) Each J_1-chain is an antiferromagnetic chain, and so is each J_2-chain.

(2) Each J_2-chain is ferromagnetically coupled to two adjacent J_2-chains via the exchange J_3 (Figure 7a).

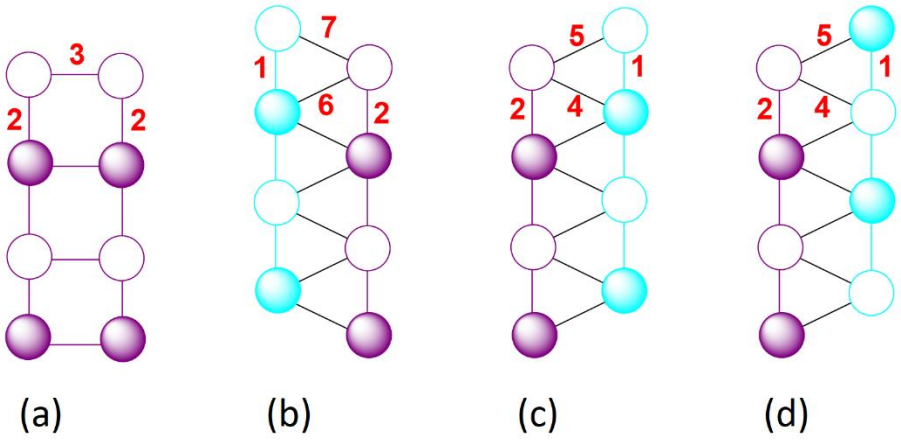

Figure 7. (**a**) Ferromagnetic coupling between two adjacent J_2-chains. (**b**) Ferromagnetic coupling between two adjacent J_1- and J_2-chains when the (J_1, J_6, J_7) and (J_2, J_6, J_7) exchange triangles are not spin-frustrated. (**c**,**d**) Two possible spin arrangements between two adjacent J_2- and J_1-chains when the (J_1, J_4, J_5) and (J_2, J_4, J_5) exchange triangles are spin-frustrated.

(3) Each J_2-chain is coupled to one J_1-chain via the antiferromagnetic exchange J_6 and the ferromagnetic exchange J_7 (Figure 7b), forming the (J_1, J_6, J_7) and (J_2, J_6, J_7) exchange triangles. With one ferromagnetic and two antiferromagnetic exchanges, each exchange triangle is not spin-frustrated, so the coupling between these J_2- and J_1-chains is ferromagnetic.

(4) Each J_2-chain is coupled to another J_1-chain via the antiferromagnetic exchanges J_4 and J_5 (Figure 7c), forming the (J_1, J_4, J_5) and (J_2, J_4, J_5) exchange triangles. With all three antiferromagnetic spin exchanges, each exchange triangle is spin frustrated. Thus, as depicted in Figure 7c,d, one can have two different spin arrangements between these J_1- and J_2-chains. This explains the presence of spin frustration in $Ba_2Mn_3(SeO_3)_6$ as indicated by its index of spin frustration of f = 5. Since J_4 is more strongly antiferromagnetic than J_5 (by a factor of approximately 3), the spin configuration of Figure 7c is energetically more stable than that of Figure 7d. The antiferromagnetic ordering at T_N = 5.7 K means that the spin configuration of Figure 7c dominates over that of Figure 7d in the population.

(5) As already noted, each J_2-chain is an antiferromagnetic chain and interacts with two adjacent J_2-chains and two adjacent J_1-chains. These interchain interactions are all

ferromagnetic except for the one with one of the two J_1-chains. The latter is spin-frustrated as described above. Above T_N = 5.7 K, where the latter spin frustration is not settled, the magnetic behavior of $Ba_2Mn_3(SeO_3)_6$ should have a strong 1D antiferromagnetic chain character because the antiferromagnetic J_1- and J_2-chains are ferromagnetically coupled (via ferromagnetic J_7 and antiferromagnetic J_6, Figure 6b). This explains the occurrence of the broad maximum in the magnetic susceptibility and the specific heat of $Ba_2Mn_3(SeO_3)_6$. However, interactions between the J_1- and J_2-chains via J_4 and J_5 are spin-frustrated, because the (J_1, J_4, J_5) and (J_2, J_4, J_5) exchange triangles are spin-frustrated so two different arrangements between the J_1- and J_2-chains are possible (Figure 6c,d).

The two sets of the spin exchanges obtained with U_{eff} = 3 and 4 eV are similar in trend. To see which set is better, one might estimate the Weiss temperature Θ using the mean field theory [21,22], to see which set leads to a value closer to the experimental value of $\Theta = -27.8$ K observed for $Ba_2Mn_3(SeO_3)_6$. According to Figure 6a,c, the Θ_{calc} value for Mn^{2+} ($S = 5/2$) ions is predicted to be

$$\Theta_{calc} = \frac{S(S+1)}{3}(2J_1 + 2J_4 + 2J_5 + 2J_6 + 2J_7), \quad (3)$$

which is –21.9 K for U_{eff} = 3 eV and –9.9 K for U_{eff} = 4 eV. Similarly, the Θ_{calc} value for Mn^{3+} ($S = 2$) ions is predicted to be

$$\Theta_{calc} = \frac{S(S+1)}{3}(2J_2 + 2J_3 + 2J_4 + 2J_5 + 2J_6 + 2J_7) \quad (4)$$

which is -10.2 K for U_{eff} = 3 eV and -1.2 K for U_{eff} = 4 eV. Thus, the spin exchanges obtained from of U_{eff} = 3 eV better describes the observed Weiss temperature.

4. Discussion and Conclusions

In summary, our magnetization and specific heat measurements of $Ba_2Mn_3(SeO_3)_6$ reveal that it is a low-dimensional antiferromagnet with a short-range one-dimensional antiferromagnetic chain behavior followed by a long-range antiferromagnetic order as marked by a succession of a broad maximum at $T_{\text{corr}} = 10.1 \pm 0.1$ K and a sharper anomaly at $T_{\text{N}} = 5.7 \pm 0.1$ K in both magnetic susceptibility (Fisher's specific heat) and specific heat. These observations are well-explained in terms of the spin exchanges of $Ba_2Mn_3(SeO_3)_6$, both antiferromagnetic and ferromagnetic, evaluated by the energy-mapping analysis. In the ordered state, $Ba_2Mn_3(SeO_3)_6$ exhibits a metamagnetic phase transition inherent for the Ising magnets with magnetization hysteresis most pronounced at low temperatures. Notably, no hysteresis is observed at $\mu_0 H = 0$ which points to the absence of spontaneous magnetization in $Ba_2Mn_3(SeO_3)_6$.

Structurally, the title compound is organized by the honeycomb layers of Mn^{3+} ions alternating with the triangular layers of Mn^{2+} ions. Magnetically, it consists of uniform chains of integer spins $S = 2$ of Mn^{3+} ions and half-integer spins $S = 5/2$ of Mn^{2+} ions running along the a axis. Qualitatively different quantum ground states, i.e., gapped and gapless spin liquid, correspondingly, can be expected for these entities [23]. However, the interaction of these chains leads to the formation of a long-range antiferromagnetic order. It would be interesting to synthesize and study isostructural phases of $Ba_2Mn_3(SeO_3)_6$ where either the divalent or the trivalent magnetic ions is replaced with nonmagnetic counterparts. The exchange interactions through a chalcogenide anion such as SeO_3^{2-} makes the scales of magnetic fields and temperatures quite convenient for experiments with equipment readily available.

While preparing this article, we became aware of an independent unpublished study on $Ba_2Mn_3(SeO_3)_6$ [24], which reported experimental data similar to ours but did not provide any theoretical analysis.

Supplementary Materials: The following supporting information can be downloaded at: https://www.mdpi.com/article/10.3390/ma16072685/s1, Figure S1: an extended view of the spin exchange paths in $Ba_2Mn_3(SeO_3)_6$. Figure S2: Eight ordered spin states used for the energy-mapping analysis.

Author Contributions: Conceptualization, A.V. and M.-H.W.; methodology, E.K.; formal analysis, A.M., S.H.C. and H.-J.K.; investigation, A.M. and E.K.; writing—original draft preparation, A.V. and M.-H.W.; writing—review and editing, A.V.; visualization, A.M.; supervision, A.V. and M.-H.W. All authors have read and agreed to the published version of the manuscript.

Funding: Support by the Megagrant program of Russian Government through project 075-15-2021-604 is acknowledged. The work at KHU was supported by the Basic Science Research Program through the National Research Foundation of Korea (NRF) funded by the Ministry of Education (2020R1A6A1A03048004).

Institutional Review Board Statement: Not applicable.

Informed Consent Statement: Not applicable.

Data Availability Statement: The data are available on reasonable request.

Conflicts of Interest: The authors declare no conflict of interest.

References

1. Greedan, J.E. Geometrically frustrated magnetic materials. *J. Mater. Chem.* **2001**, *11*, 37–53. [CrossRef]
2. Xiang, H.; Lee, C.; Koo, H.-J.; Gong, X.; Whangbo, M.-H. Magnetic properties and energy-mapping analysis. *Dalton Trans.* **2013**, *42*, 823–853. [CrossRef] [PubMed]
3. Whangbo, M.-H.; Xiang, H.J. Magnetic properties from the perspectives of electronic Hamiltonian: Spin exchange parameters, spin orientation and spin-half misconception. In *Handbook in Solid State Chemistry, Volume 5: Theoretical Descriptions*; Dronskowski, R., Kikkawa, S., Stein, A., Eds.; Wiley: New York, NY, USA, 2017; pp. 285–343.
4. Whangbo, M.-H.; Koo, H.-J.; Kremer, R.K. Spin exchanges between transition metal ions governed by the ligand p-orbitals in their magnetic orbitals. *Molecules* **2021**, *26*, 531. [CrossRef] [PubMed]
5. Xiang, H.J.; Whangbo, M.-H. Density functional characterization of the multiferroicity in spin spiral chain cuprates. *Phys. Rev. Lett.* **2007**, *99*, 257253. [CrossRef] [PubMed]
6. Boidi, N.A.; Helman, C.; Nunez-Fernandez, Y.; Hallberg, K.; Aligia, A.A. Determination of superexchange interactions for the CuO_2 chains in $LiCu_2O_2$. *Phys. Rev. B* **2023**, *107*, 085128. [CrossRef]
7. Isobe, M.; Ueda, Y. Magnetic susceptibility of quasi-one-dimensional compound α'-NaV_2O_5—Possible spin-Peierls compound with high critical temperature of 34 K. *J. Phys. Soc. Jpn.* **1996**, *65*, 1178–1181. [CrossRef]
8. Zhang, W.; Cui, M.; Tian, J.; Jiang, P.; Qian, G.; Lu, X. Two magnetic orderings and a spin-flop transition in mixed valence compound $Mn_3O(SeO_3)_3$. *Materials* **2022**, *15*, 5773. [CrossRef] [PubMed]
9. Ishiwata, S.; Bos, J.W.G.; Huang, Q.; Cava, R.J. Structure and magnetic properties of hollandite $Ba_{1.2}Mn_8O_{16}$. *J. Phys. Condens. Matter* **2006**, *18*, 3745–3752. [CrossRef]
10. Johnston, M.G.; Harrison, W.T.A. Two new octahedral/pyramidal frameworks containing both cation channels and lone-pair channels: Syntheses and structures of $Ba_2Mn^{II}Mn_2^{III}(SeO_3)_6$ and $PbFe_2(SeO_3)_4$. *J. Sol. St. Chem.* **2004**, *177*, 4680–4686. [CrossRef]
11. Koo, H.-J.; Kremer, R.; Whangbo, M.-H. Unusual spin exchanges mediated by the molecular anion $P_2S_6^{4-}$: Theoretical analyses of the magnetic ground states, magnetic anisotropy and spin exchanges of MPS_3 (M = Mn, Fe, Co, Ni). *Molecules* **2021**, *26*, 1410. [CrossRef] [PubMed]
12. Zener, C. Interaction between the d-shells in the transition metals. II. Ferromagnetic compounds of manganese with perovskite structure. *Phys. Rev.* **1951**, *82*, 403–405. [CrossRef]
13. Bain, G.A.; Berry, J.F. Diamagnetic corrections and Pascal's constants. *J. Chem Educ.* **2008**, *85*, 532–536. [CrossRef]
14. Blundell, S. *Magnetism in Condenced Matter*; Oxford University Press: Oxford, UK, 2001; 272p.
15. Markina, M.; Vasilchikova, T.; Kuznetsova, E.; Berdonosov, P.; Olenev, A.; Chung, S.H.; Koo, H.-J.; Whangbo, M.-H.; Vasiliev, A. Preparation and characterization of francisite solid solutions $Cu_3Bi(Se_{1-x}Te_xO_3)_2O_2Br$ (x = 0–1): Possibility for francisites as starting materials for oxide van der Waals Ferromagnets. *Chem. Mater.* **2023**, *35*, 511–520. [CrossRef]
16. Blöchl, P.E. Projector augmented-wave method. *Phys. Rev. B* **1994**, *50*, 17953–17979. [CrossRef] [PubMed]
17. Kresse, G.; Joubert, D. From ultrasoft pseudopotentials to the projector augmented-wave method. *Phys. Rev. B* **1999**, *59*, 1758–1775. [CrossRef]
18. Kresse, G.; Furthmüller, J. Efficient iterative schemes for ab initio total-energy calculations using a plane-wave basis set. *Phys. Rev. B* **1996**, *54*, 11169–11186. [CrossRef] [PubMed]
19. Perdew, J.P.; Burke, K.; Ernzerhof, M. Generalized gradient approximation made simple. *Phys. Rev. Lett.* **1996**, *77*, 3865–3868. [CrossRef] [PubMed]
20. Dudarev, S.L.; Botton, G.A.; Savrasov, S.Y.; Humphreys, C.J.; Sutton, A.P. Electron-energy-loss spectra and the structural stability of nickel oxide: An LSDA+U study. *Phys. Rev. B* **1998**, *57*, 1505–1509. [CrossRef]

21. Lee, K.H.; Lee, J.Y.; Lee, C.; Whangbo, M.-H. Evaluating the Curie-Weiss temperature of a magnetic system composed of nonequivalent magnetic ions in terms of spin exchange constants. *Bull. Korean Chem. Soc.* **2014**, *35*, 1277–1278. [CrossRef]
22. Smart, S.J. *Effective Field Theory of Magnetism*; Saunders: Philadelphia, PA, USA, 1966.
23. Vasiliev, A.; Volkova, O.; Zvereva, E.; Markina, M. Milestones of low-D quantum magnetism. *NPJ Quant. Mater.* **2018**, *3*, 18. [CrossRef]
24. Lu, C.; Zhang, Y.; Cui, M.; Zhao, Z.; He, Z. Synthesis and Magnetic Properties of Two Mixed-Valence Compounds a $2Mn^{II}Mn_2{}^{III}(SeO_3)_6$ (A = Sr and Ba). SSRN. Available online: https://ssrn.com/abstract=4355499 (accessed on 12 February 2023).